



RESEARCH MEMORANDUM

for

U. S. Army Ordnance

A LOW-SPEED INVESTIGATION OF THE MAGNUS EFFECTS ON A
STING-MOUNTED MODEL OF A TYPICAL MORTAR SHELL

By Jacob H. Lichtenstein

Langley Aeronautical Laboratory
Langley Field, Va.

CLASSIFICATION CHANGED TO DECLASSI-
FIED EFFECTIVE JUNE 12, 1963
AUTHORITY NASA 1.1-4 BY J. J. CARROLL


The material contained in this report is the property of the National Advisory Committee for Aeronautics and is loaned to your agency. It and its contents are not to be distributed outside your agency without the express written permission of the National Advisory Committee for Aeronautics. This prohibition is in any event not to be construed as meaning that the material is to be kept secret or classified in any way.

**NATIONAL ADVISORY COMMITTEE
FOR AERONAUTICS**
WASHINGTON

CONFIDENTIAL

NATIONAL ADVISORY COMMITTEE FOR AERONAUTICS

RESEARCH MEMORANDUM

for

U. S. Army Ordnance

A LOW-SPEED INVESTIGATION OF THE MAGNUS EFFECTS ON A
STING-MOUNTED MODEL OF A TYPICAL MORTAR SHELL

By Jacob H. Lichtenstein

SUMMARY

An investigation has been made in the Langley stability tunnel with a 2.5-scale spinning model of a typical mortar shell. These tests were made to measure the aerodynamic forces and moments acting on a typical spinning mortar shell.

It was found that the Magnus moments varied nonlinearly with angle of attack and that their magnitude became important above angles of attack of about 10° . The model exhibited directional instability up to moderate angles of attack; thus, the possibility of large angular deflections being attained after a disturbance are indicated. This combined with the nonlinear Magnus moments could result in a large-amplitude precessional motion.

Enclosing the tail fins in a shroud increased the directional stability of the model. Pointing the nose of the model tended to increase, and flattening the nose tended to decrease, the Magnus effects.

INTRODUCTION

The problem of the short-round behavior (wherein an occasional round falls far short of its intended range) in the firing of mortar shells has been of considerable concern for some time, and therefore both analytical and experimental investigations have been undertaken to explore this problem. (See, for example, refs. 1 to 6.) These investigations in general have shown that an instability of spin when coupled with other influences such as destabilizing Magnus effects can, if there is a sufficiently large disturbance in yaw, result in a large-amplitude precessional

motion which in turn causes the short-round performance. The dynamic-stability investigation of reference 5 showed the existence of this instability for the mortar shell investigated herein.

The purpose of this investigation was to determine the magnitude of the aerodynamic forces and moments, particularly the Magnus moment, acting on a typical mortar shell with and without spin. The tests were made on the sting-support system of the Langley stability tunnel. The model was a 2.3-scale model of a typical mortar shell which was spun at speeds from 0 to 600 rpm for angles of attack from -4° to $+27^{\circ}$. During the course of testing, some modifications were made to the nose and tail of the model to find the influence of sharp and flat nose shapes and of shrouding the tail fins or reducing the number of fins on the tail.

SYMBOLS

The data presented herein are in the form of standard coefficients and symbols about a body axis system which is shown in figure 1. The moment center was the center of gravity of the model. The symbols used are defined as follows:

C_N	normal-force coefficient, $\frac{F_N}{qA}$
C_Y	side-force coefficient, $\frac{F_Y}{qA}$
C_n	yawing-moment coefficient, $\frac{M_Z}{qAl}$
C_m	pitching-moment coefficient, $\frac{M_Y}{qAl}$
C_l	rolling-moment coefficient, $\frac{M_X}{qAl}$
F_N	normal force, lb
F_Y	side force, lb
M_X	rolling moment about X-axis, ft-lb
M_Y	pitching moment about Y-axis, ft-lb
M_Z	yawing moment about Z-axis, ft-lb

q dynamic pressure, $\frac{1}{2}\rho V^2$, lb/sq ft

ρ mass density of air, slugs/cu ft

V velocity, ft/sec

A cross-sectional area, $\frac{\pi}{4} d^2$, sq ft

l length, ft

d diameter, ft

$\frac{pl}{2V}$ nondimensional rolling parameter of X body axis about
 X wind axis (rate of precession)

p rolling velocity of X body axis about X wind axis, radians
per sec

X, Y, Z body axes

X_w, Z_w X and Z wind axes

α angle of attack, same as angle of yaw for symmetrical missile,
deg

$$C_{n_p} = \frac{\partial C_n}{\partial \left(\frac{pl}{2V} \right)}$$

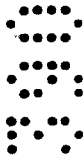
$$C_{l_p} = \frac{\partial C_l}{\partial \left(\frac{pl}{2V} \right)}$$

$$C_{Y_p} = \frac{\partial C_Y}{\partial \left(\frac{pl}{2V} \right)}$$

$$C_{m_p} = \frac{\partial C_m}{\partial \left(\frac{pl}{2V} \right)}$$

$$C_{n_p} = \frac{\partial C_N}{\partial \left(\frac{pl}{2V} \right)}$$

APPARATUS, MODELS, AND TESTS



The model used in the present investigation was a 2.3-scale model of a typical 81-mm mortar shell. A sketch of the model with pertinent dimensions is shown in figure 2 along with a sketch of an antisubmarine-rocket model. In addition to the original nose, three modified nose configurations were used (see figs. 3 and 4): a pointed-nose missile obtained by installing a pointed nose on the end of the original nose, a blunt-nose missile obtained by installing a flat plate on the model after removal of 7.5 inches of the original missile nose, and a missile with a nose-ring spoiler was simulated with a 7-inch-diameter ring made of 1/8-inch-diameter tubing and located 8.89 inches rearward of the flat of the original nose. Three different tail-fin arrangements were tested: the original 12-fin tail, a similar 6-fin tail, and a 12-fin tail with a shroud (fig. 5).

The basic model was constructed of a spun-magnesium skin 1/16 inch thick with aluminum bulkheads at the front and rear of the motor drive mechanism. For strength, turned aluminum parts were used at the nose, at the station where the conical nose separates from the front of the model, at the grooved section where the rear conical section begins, and at the juncture of the rear conical section and the tail boom. The tails were made of balsa in order to keep the model as light as possible. The entire model was dynamically balanced to maintain the out-of-balance dynamic forces as small as possible.

The model was mounted on the sting-support system in the Langley stability tunnel as shown in figure 6. The sting proper was supported by two lead screws in the pylon. Changes in the angle of attack were achieved by operating the two screws differentially so that the center of gravity of the model had no appreciable vertical movement. An exploded view of the mounting mechanism and model is shown in figure 7. The sting, strain gage, and motor drive mechanism are shown in the relative axial positions they would actually have when assembled. The trailing wires were brought out through a hole in the sting. The drive motor was an air-cooled variable-frequency motor, and among the bundle of wires was a tube which supplied cooling air for the motor. Spin was transmitted to the model by the drive plate which was attached to a bulkhead in the forward section of the model. The rotational velocity of the model was controlled by varying the frequency of the voltage to the drive motor. A Strobocoenn scanning unit in conjunction with the generator mounted on the drive mechanism was used to determine the spin rate.

The strain gage was a five-component gage measuring normal force, side force, pitching moment, yawing moment, and rolling moment. The output from the strain gage was fed to printing heads of the mechanical-balance system in the Langley stability tunnel.

The tests were made at a dynamic pressure of 24.9 pounds per square foot which corresponds to a Mach number of 0.13 and a Reynolds number of 4×10^6 based upon the model length. The angle of attack was varied from -4° to $+27^\circ$ in 4° increments except the last. Tests were made at spin rates of 0, 200, 400, and 600 rpm for the basic configuration and only 0 and 600 rpm for the others. For the basic configuration the rolling-flow technique of the stability tunnel was utilized to measure the aerodynamic loads due to a precessional type of motion for the various spin rates. A list of the tests is given in table I.

CORRECTIONS

Because of the small lift developed by the missile and the small area relative to the tunnel, no corrections for jet boundary or blockage were applied. Neither were corrections applied for the effects of turbulence or sting-support interference.

RESULTS AND DISCUSSION

Presentation of Data

The data for the original configuration are presented in figures 8 and 9 for straight flow and rolling flow, respectively. Data are shown for the original configuration with the 6-fin tail in figure 10 and the 12-fin tail with the shroud in figure 11. The data for the different nose configurations are presented in the following figures: figure 12 for the pointed nose and original tail, figure 13 for the pointed nose and 6-fin tail, figure 14 for the flat nose and original tail, and figure 15 for the original nose with a ring spoiler and original tail. A comparison of the Magnus effects of the original configuration with those configurations which had the largest and smallest Magnus effects is presented in figure 16. A comparison of the present data for the mortar shell and the data from reference 7 for an antisubmarine rocket is made in figure 17.

DISCUSSION

Basic Configuration

The straight-flow data for the basic configuration (fig. 8) show that the yawing-moment coefficient C_n , which is representative of the Magnus moment for the spinning model, varies nonlinearly with angle of

attack for all of the spin rates tested. For angles of attack up to about 10° the moment is small and the effect of spin is practically nonexistent. Above $\alpha = 10^\circ$, however, spin introduces a positive yawing moment whose magnitude increases with the spin rate. Limitations of the equipment restricted tests to a maximum angle of attack of 27° and spin rates to 600 rpm. Inasmuch as the Magnus moment was still increasing with spin rate and angle of attack, the limitations of the equipment therefore prevented attainment of maximum values for the Magnus moments.

The side-force coefficient C_y due to spinning, which represents the Magnus forces, exhibits characteristics similar to those for the yawing moment but in a negative direction. The fact that the side force and yawing moment are of opposite signs indicates that the center of pressure for the Magnus forces is behind the center of gravity. For most cases it appears to be about 0.2 length of the body rearward of the center of gravity.

The magnitude of the rolling-moment coefficient C_l increased in a negative direction as the angle of attack increased for all the spin rates. This increase in magnitude of the rolling moment indicates the presence of some asymmetry of the model or airstream. The rate of spin apparently has only a minor effect on C_l .

The pitching-moment coefficient C_m data (which, in this case, describe the static stability in both pitch and yaw) show an unstable variation with angle of attack up to about 16° . Above 16° the pitching-moment curve becomes stable with a stable trim point occurring between 20° and 24° . This instability permits attainment of large angles of attack (or yaw) where the Magnus effects are large and can help maintain a large-amplitude precessional motion. This behavior would result in a high drag and consequential loss in range. The static stability of the model generally showed a slight improvement as the spin rate increased.

The normal-force coefficient C_N increased regularly with angle of attack and there were only minor effects of rate of spin.

The rolling-flow tests (fig. 9) simulate a precessional motion in which the amplitude of the motion is given by the angle of attack of the model. Inasmuch as the C_{l_p} term is practically zero for the angles of attack tested, the damping of the precessional motion is given by $C_{n_p} \sin \alpha$. The data indicate that the damping increases at the higher angles of attack where it is necessary, and also that the damping generally increases with spin rate. The pitching-moment coefficient and normal-force coefficient due to precession were practically zero throughout the angle of attack for the no-spin condition, and increased in magnitude as the spin rate increased. The pitching moment increased in a manner to aid the static stability of the model.

The tests were limited to an angle of yaw below that for which instability was obtained in the tests of reference 5; nevertheless, some interesting observations can be made. The lack of static stability in yaw for the mortar shell shown by the present test indicates that relatively minor disturbances can induce fairly large angles of yaw. At a large angle of yaw, where the data of reference 5 indicated that instability of spin can develop, a spinning motion will introduce large yawing moments. This combination could result in a large-amplitude precessional motion with an attendant decrease in range. It appears, therefore, that some manner of insuring that only small angles of yaw would be encountered in flight, such as increasing the tail area or of eliminating the large Magnus moments of the spinning shell, would be necessary to maintain the desired stability.

Effect of Changes in Tail Configuration

The effect of some changes in the tail configuration can be seen by comparison of the data in figure 8 for the basic model with those of figure 10 for the 6-fin tail and figure 11 for the 12-fin tail with shroud. Although the data in reference 5 indicated that the 6-fin-tail configuration was somewhat less stable than the basic configuration, the data in figure 10 show only minor effects of this change in tail configuration for the angle-of-attack range investigated. The change to the tail with a shroud generally produced little effect on all but the pitching moment (fig. 11). In this case, the variation was stable over the entire angle-of-attack range. This should reduce the tendency of the missile to wallow up to moderate deflections after a minor disturbance.

Effect of Changes in the Nose Configuration

The changes made at the nose of the model generally produced larger effects on the Magnus moment than the changes made at the tail. Pointing the nose tended to increase the Magnus moment as can be seen by comparison of data in figure 12 with that presented previously in figure 8. Flat-tening the nose however, tended to decrease the Magnus moments. (Compare data in fig. 14 with fig. 8.) This effect is shown in figure 16 to some extent where the basic configuration is compared with a flat-nose configuration and a pointed-nose and 6-fin-tail configuration. These data are in agreement with the dynamic-test data of reference 5 wherein it was found that the pointed-nose 6-fin-tail configuration was the most unstable and the flat-nose model somewhat more stable than the original configuration. However, these changes did not have the desirable effect of eliminating the Magnus moment.

The effect of adding a nose ring to the original configuration was negligible. (Compare fig. 15 with fig. 8.)

Comparison of Mortar Shell and Antisubmarine Rocket

The data presented in figure 17 are a comparison of the present results for the mortar shell and the results of an antisubmarine rocket (from ref. 7) at a spin rate of 600 rpm. This antisubmarine rocket experienced a type of instability similar to that of the mortar shell in that, for the spinning rocket, a deflection to a large angle of attack was followed by a large-amplitude precessional motion which seriously decreased the range.

The data in figure 17 show that both configurations have similar Magnus effects in that the variation with angle of attack is decidedly nonlinear and increases rapidly at angles above some moderate value. The static stability in yaw C_m is considerably better for the antisubmarine rocket than the mortar shell even with the shrouded tail, probably because the smoother shape of the antisubmarine rocket allows more effective air flow at the fins.

CONCLUSIONS

The results of a wind-tunnel investigation of a typical mortar shell mounted on a sting support and free to spin indicate the following conclusions:

1. For the basic configuration, the Magnus moments varied nonlinearly with angle of attack. These moments were relatively unimportant below an angle of attack of 10° but above this angle they increased rapidly.
2. The directional instability exhibited by the model up to angles of attack of 16° indicated the possibility of attaining large angles of yaw. At these large angles the Magnus moment is big and this combination could lead to the development of a large-amplitude precessional motion with an attendant decrease in range.
3. Enclosing the tail fins in a shroud increased the directional stability so that the configuration was stable over the entire angle-of-attack range tested.

4. Changes at the nose of the model seemed to have greater effects on the Magnus moment than changes at the tail. Pointing the nose tended to increase, and flattening the nose tended to decrease, the Magnus effects.

Langley Aeronautical Laboratory,
National Advisory Committee for Aeronautics,
Langley Field, Va., December 6, 1956.

Jacob H. Lichtenstein
Jacob H. Lichtenstein
Aeronautical Research Engineer

Approved:

Charles H. Zimmerman
for Thomas A. Harris
Chief of Stability Research Division

mhg

REFERENCES

1. Zaroodny, Serge J.: On the Mechanism of Dispersion and Short Ranges of Mortar Fire. With an Appendix on an Alternate Solution of the Equations of Motion of a Yawing Projectile - Rep. No. 668, Ballistic Res. Labs., Aberdeen Proving Ground, Apr. 7, 1948.
2. Zaroodny, Serge J.: On the Dispersion and Short Ranges of Mortar Fire. Memo. Rep. No. 685, Ballistic Res. Labs., Aberdeen Proving Ground, July 1953.
3. Zaroodny, Serge J.: Failure of the Instability of Spin of the First Kind. Memo. Rep. No. 832, Ballistic Res. Labs., Aberdeen Proving Ground, Sept. 1954.
4. Schmidt, J. M.: Analog Computer Simulation of Flight Characteristics of Two 90 MM Fin Stabilized Shell T108E40 and T316. Memo. Rep. No. 953, Ballistic Res. Labs., Aberdeen Proving Ground, Dec. 1955.
5. Bird, John D., and Lichtenstein, Jacob H.: An Investigation of a Source of Short-Round Behavior of Mortar Shells. NACA RM L56G20a, 1956.
6. Bird, John D., and Lichtenstein, Jacob H.: Wind-Tunnel Experiments Concerning the Dynamic Behavior of a Low-Speed Slowly Spinning Fin-Stabilized Rocket. NACA RM L54D22, 1954.
7. Lichtenstein, Jacob H.: A Wind-Tunnel Investigation of the Effect of Nose Ring Spoilers on a Low-Speed Slowly Spinning Fin-Stabilized Rocket. NACA RM SL56G16, U. S. Army Ordnance, 1956.

TABLE I

TESTS AND DATA FIGURES

Configuration			Type of data	Data in figure -
Number	Nose	Tail		
1	Original	Original	Straight flow	8
1	Original	Original	Rolling flow	9
2	Original	6-fin	Straight flow	10
3	Original	12-fin with shroud	Straight flow	11
4	Pointed	Original	Straight flow	12
5	Pointed	6-fin	Straight flow	13
6	Flat	Original	Straight flow	14
7	Original and ring spoiler	Original	Straight flow	15
Comparison of configurations 1, 5, and 6			Straight flow	16
Comparison of configuration 1 and antisubmarine rocket			Straight flow	17

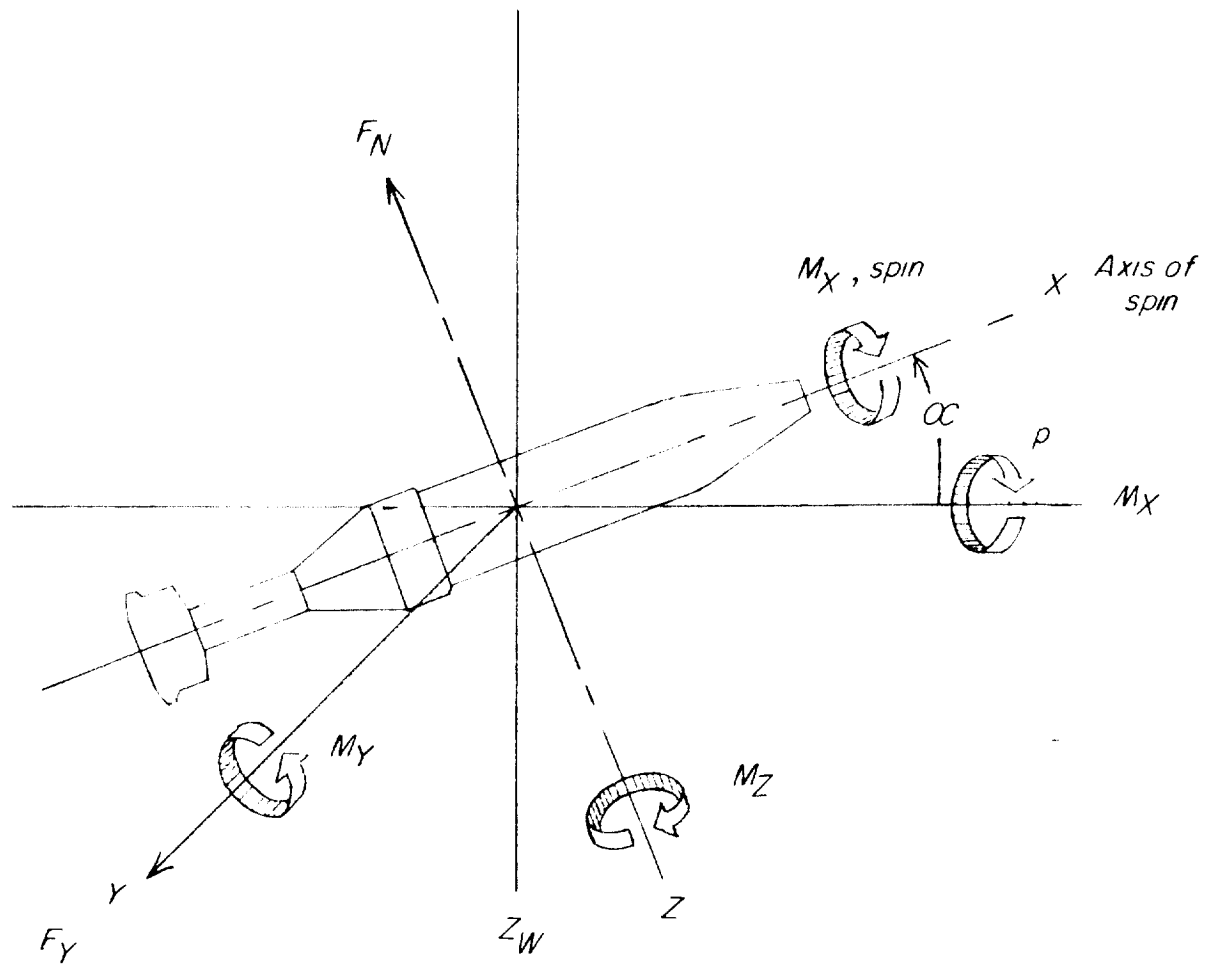


Figure 1.- System of axes used. Arrows indicate positive direction of forces, moments, angles, and angular velocities.

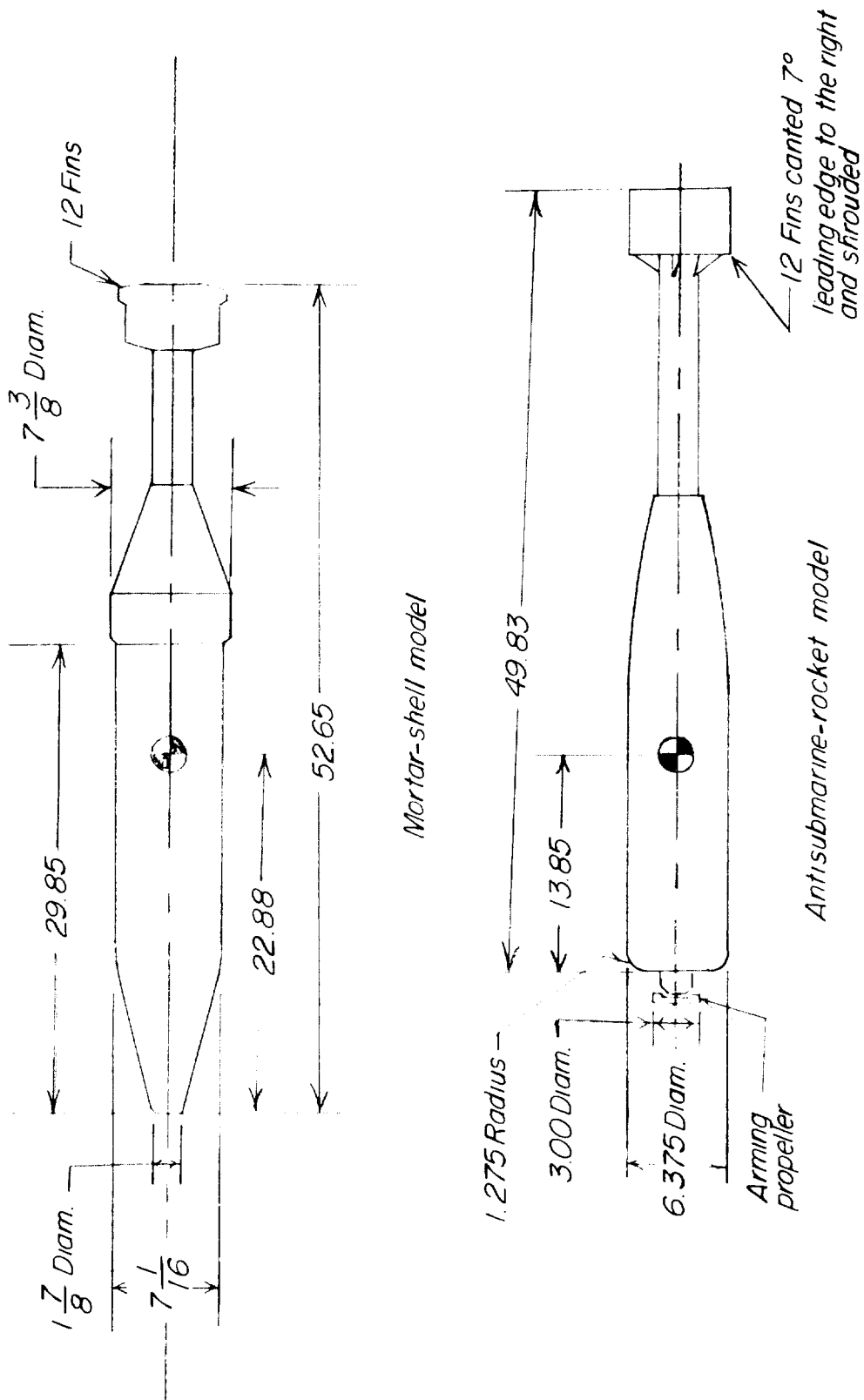


Figure 2.- Sketches of mortar-shell model used in the tests, and of antisubmarine-rocket model for comparison. All dimensions are in inches.

23



Original nose cone which
was removed for flat-
nose tests

Flat plate installed on
model for flat-nose
tests

Pointed nose installed on
end of original nose

Figure 3.- Nose configurations tested.

L-93095

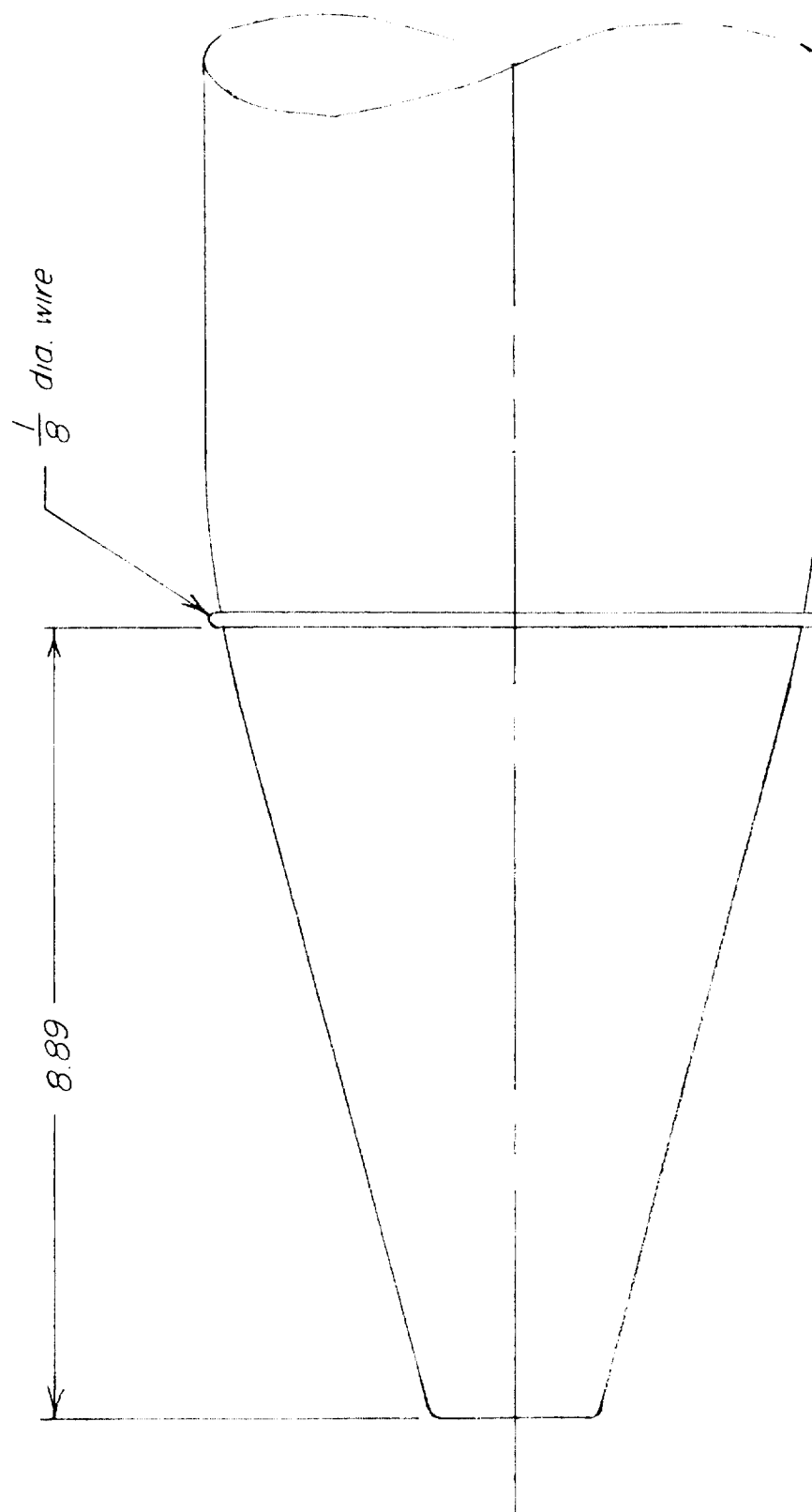


Figure 4.- Sketch showing location of ring spoiler. Dimensions are in inches.

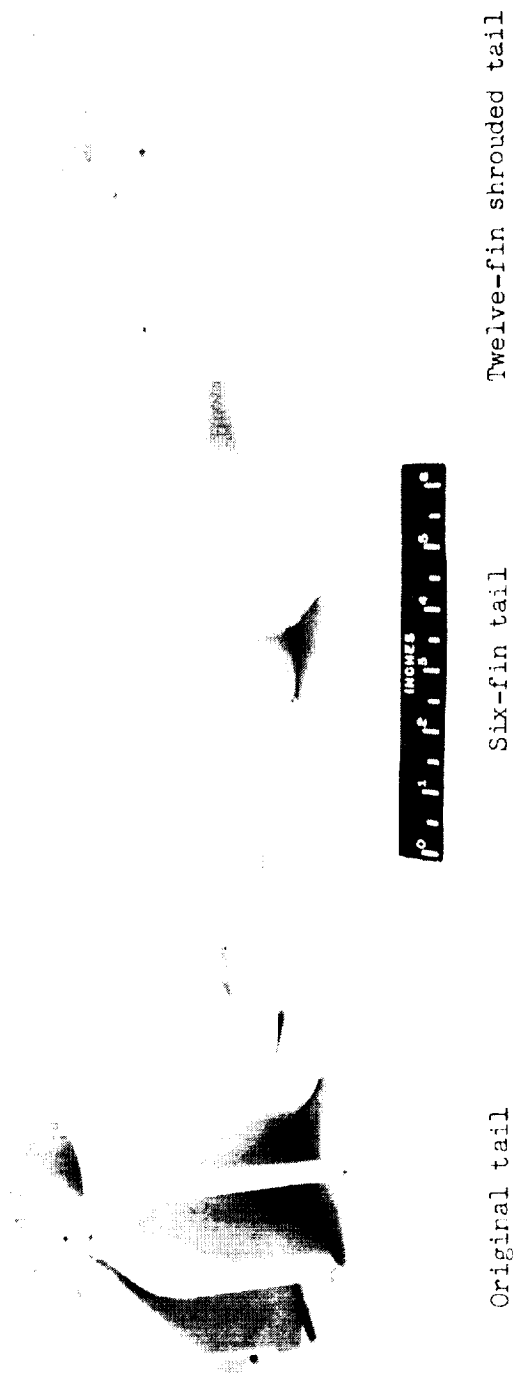
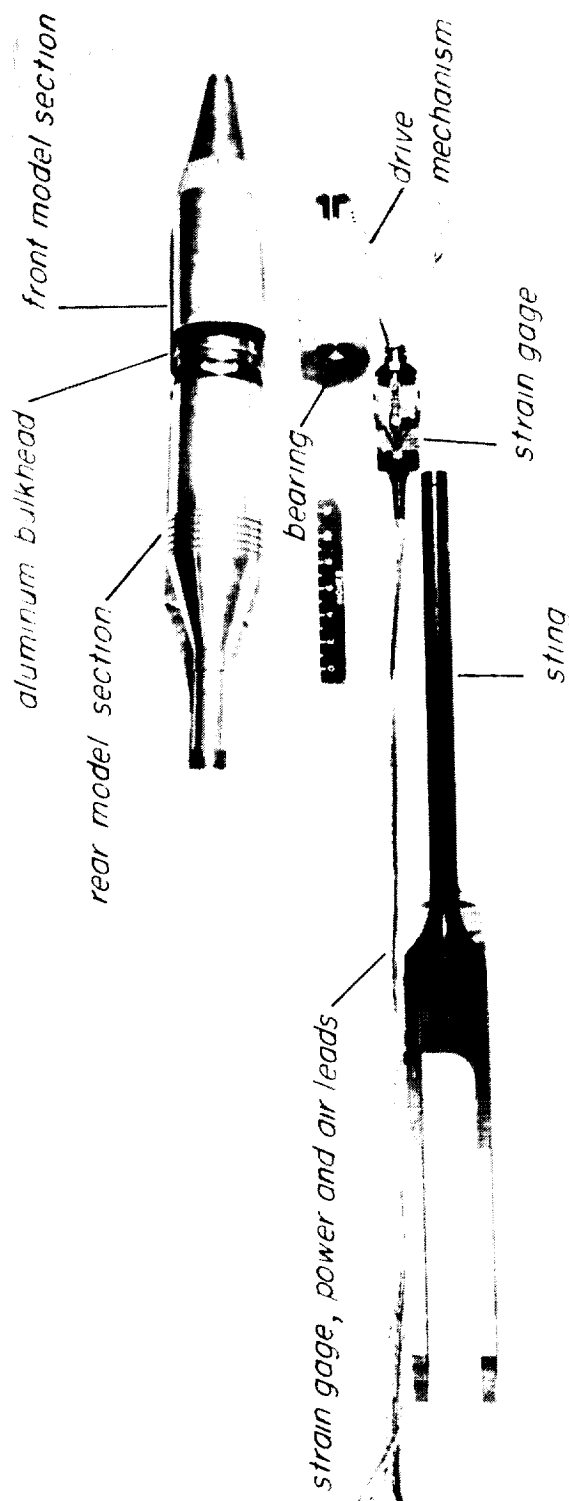


Figure 5.- Tail configurations tested. L-93096



Figure 6.- Photograph showing the sting-support system in the Langley stability tunnel.

L-93094



L-93129
Figure 7.- Photograph showing exploded view of sting, strain gage, drive mechanism, and of model.

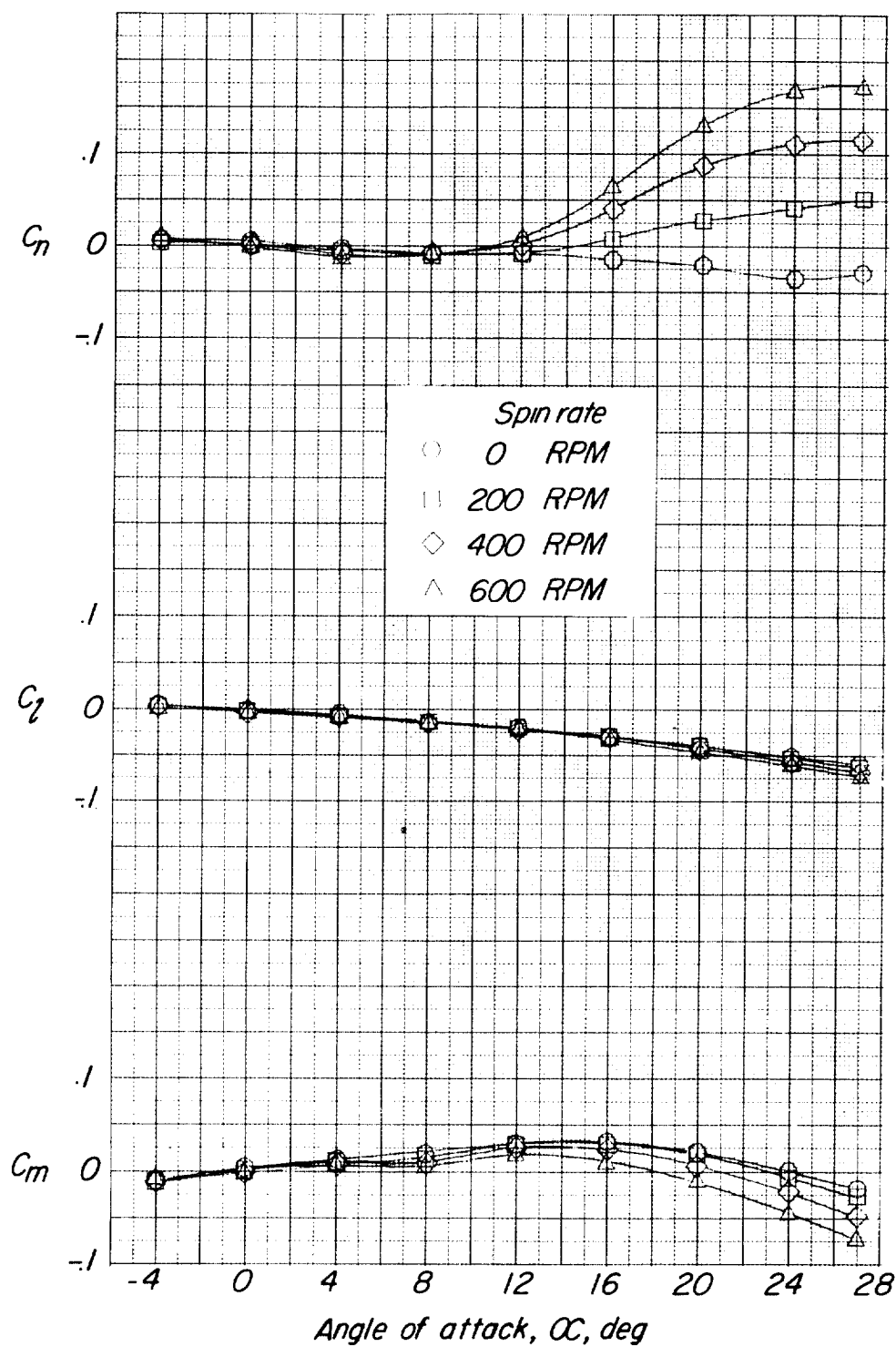


Figure 8.- Variation of the measured forces and moments against angle of attack in straight flow for various spin rates for the original configuration (original nose, original tail).

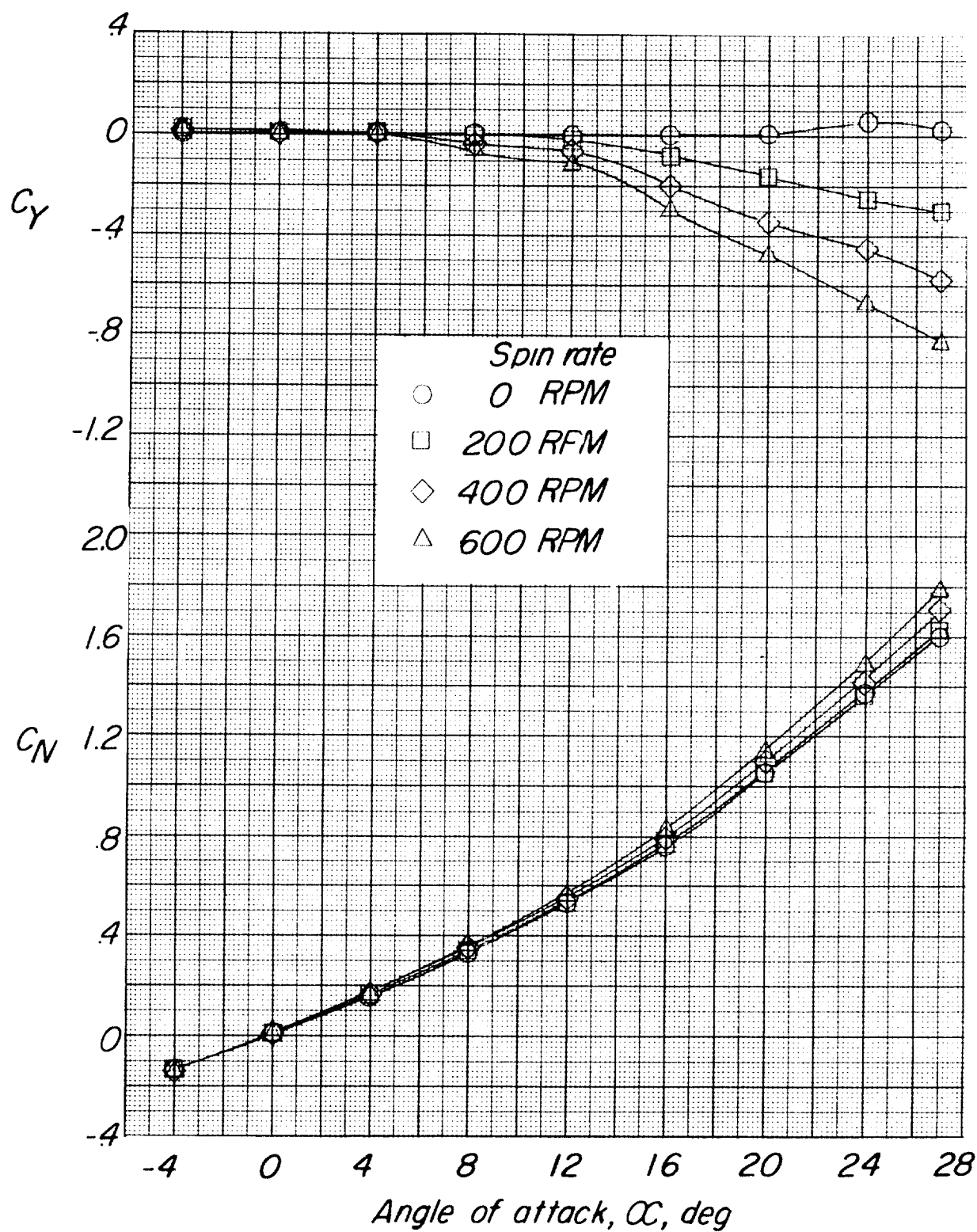


Figure 8.- Concluded.

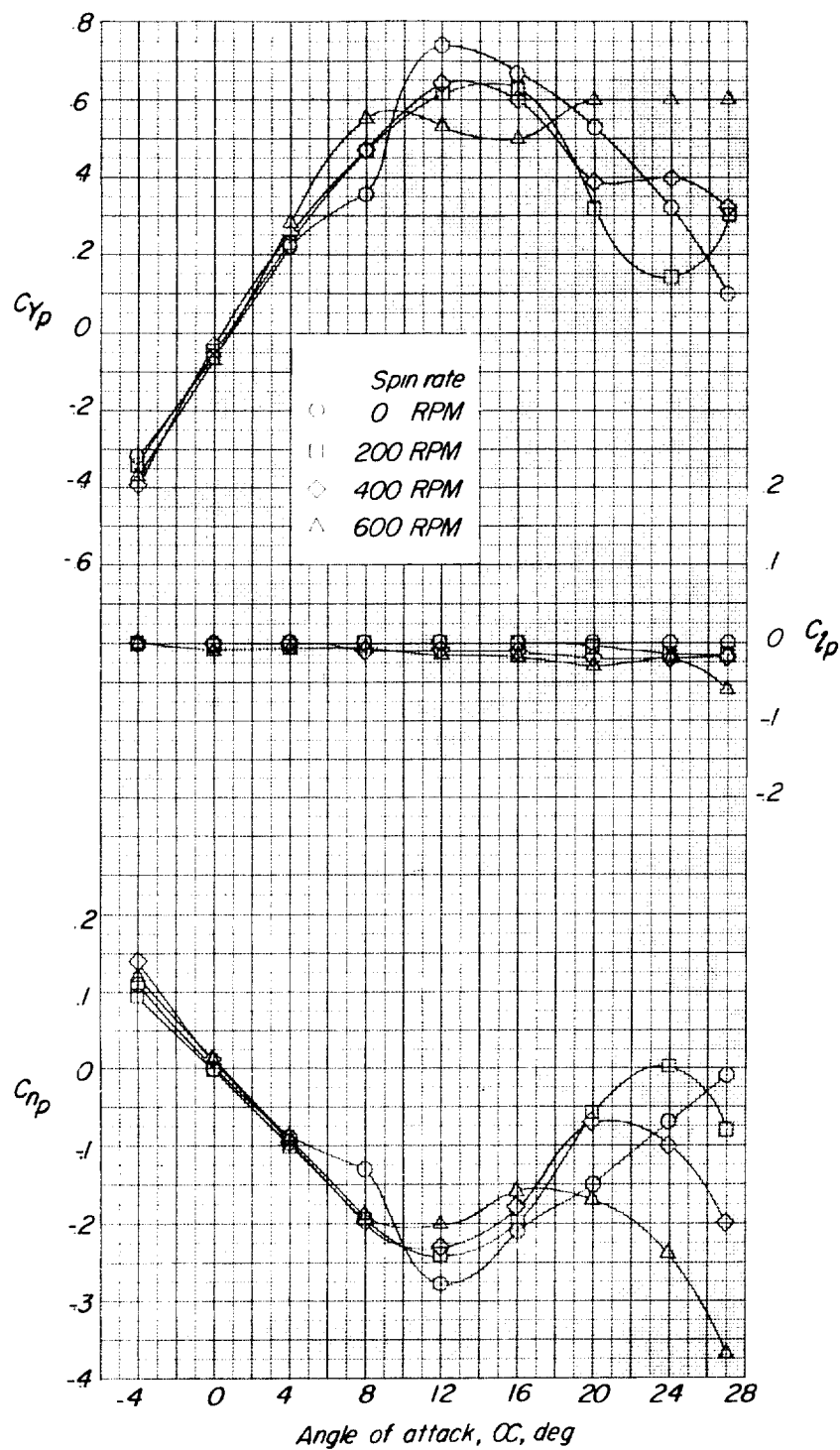


Figure 9.- Variation of the measured forces and moments against angle of attack in rolling flow for various spin rates for the original configuration (original nose, original tail).

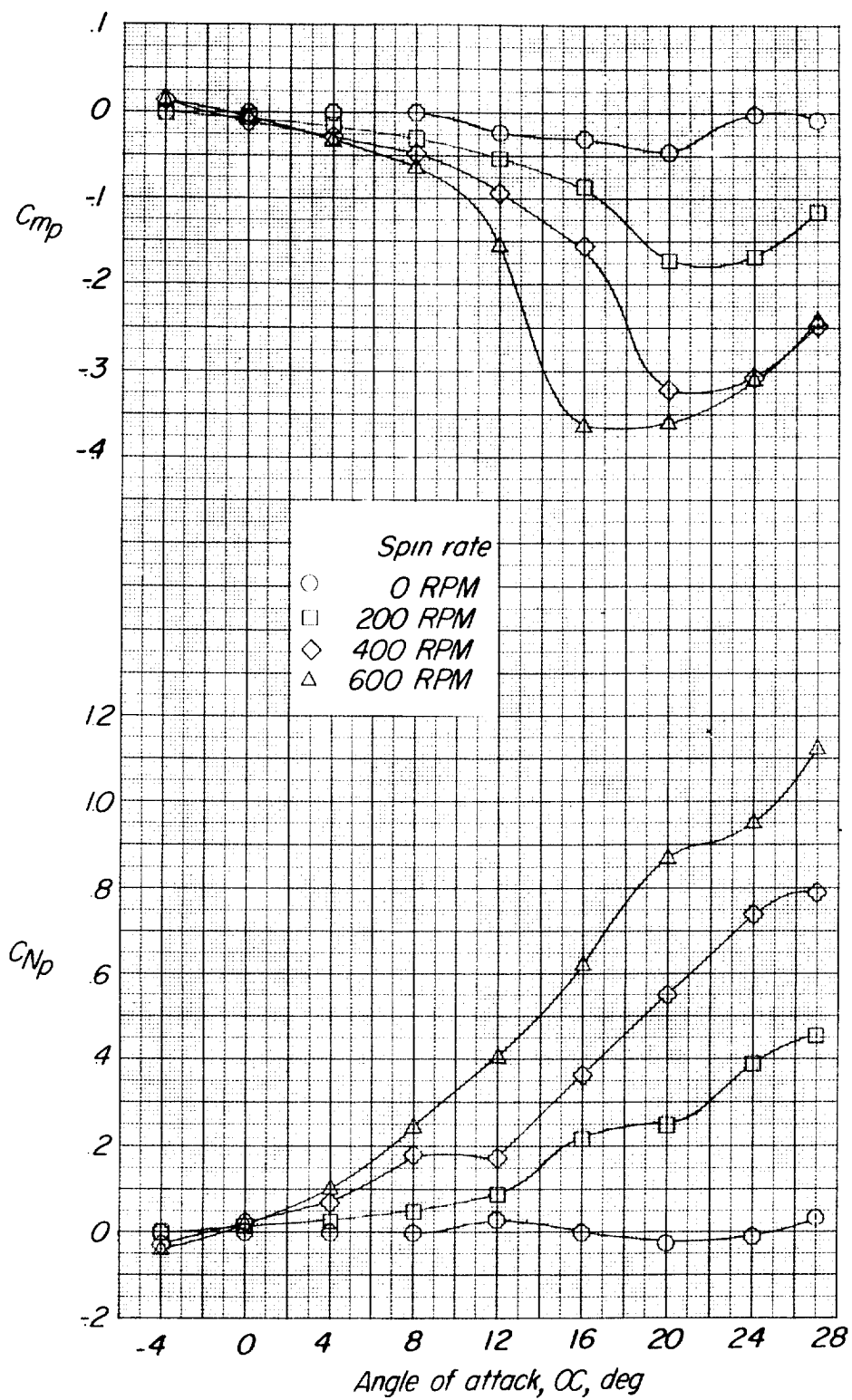


Figure 9.- Concluded.

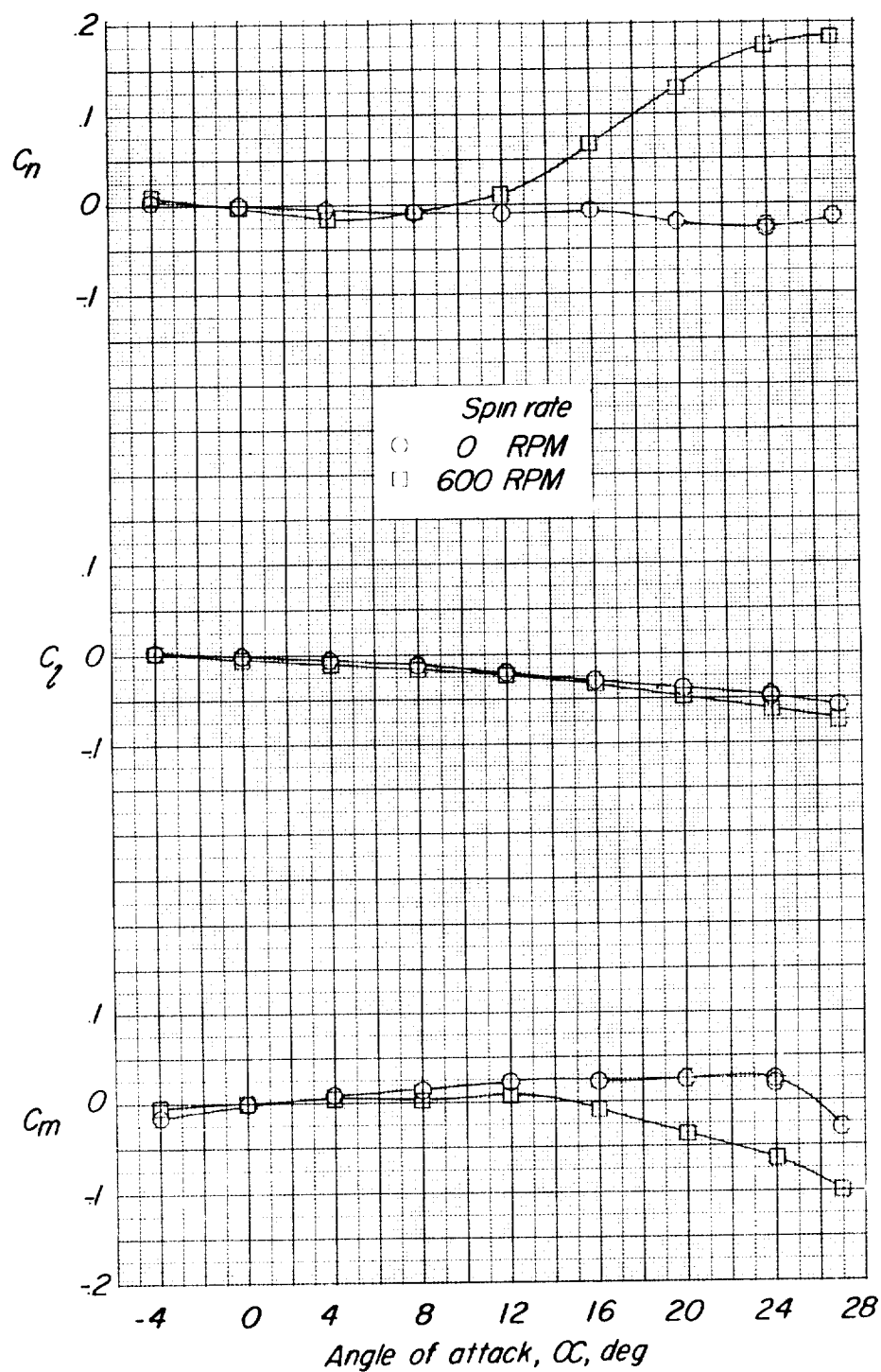


Figure 10.- Variation of the measured forces and moments against angle of attack in straight flow for two spin rates for the configuration with original nose and 6-fin tail.

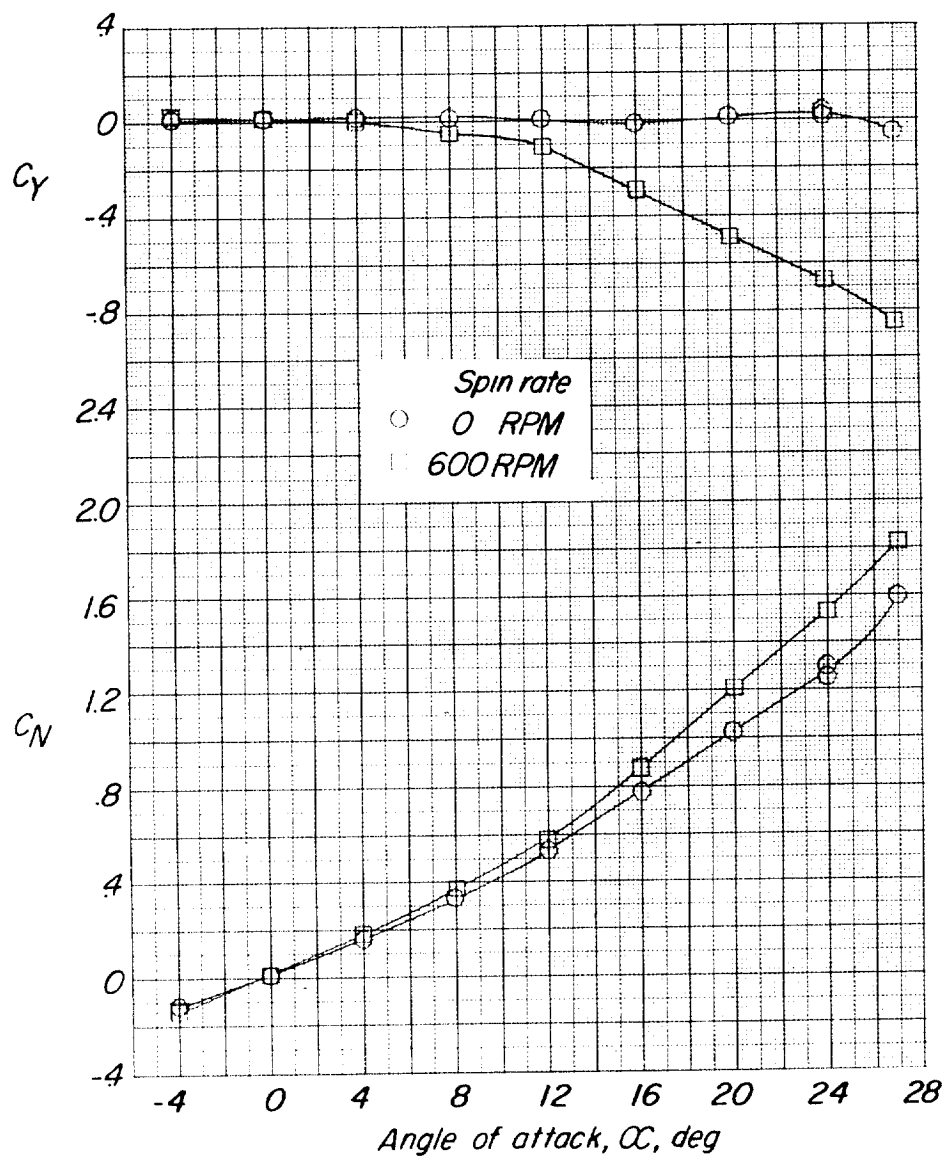


Figure 10.- Concluded.

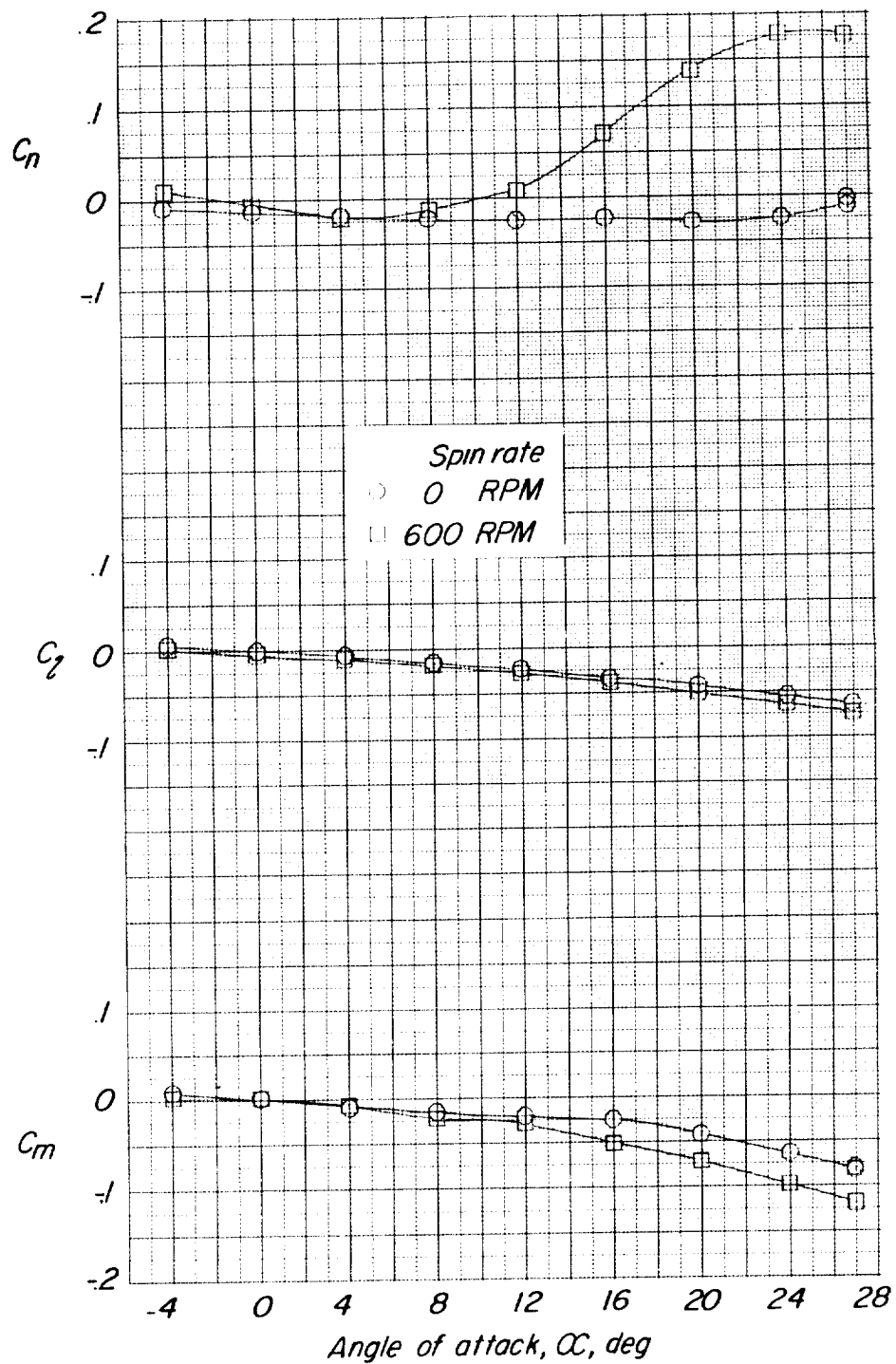


Figure 11.- Variation of the measured forces and moments against angle of attack in straight flow for two spin rates for the configuration with original nose and 12-fin tail with shroud.

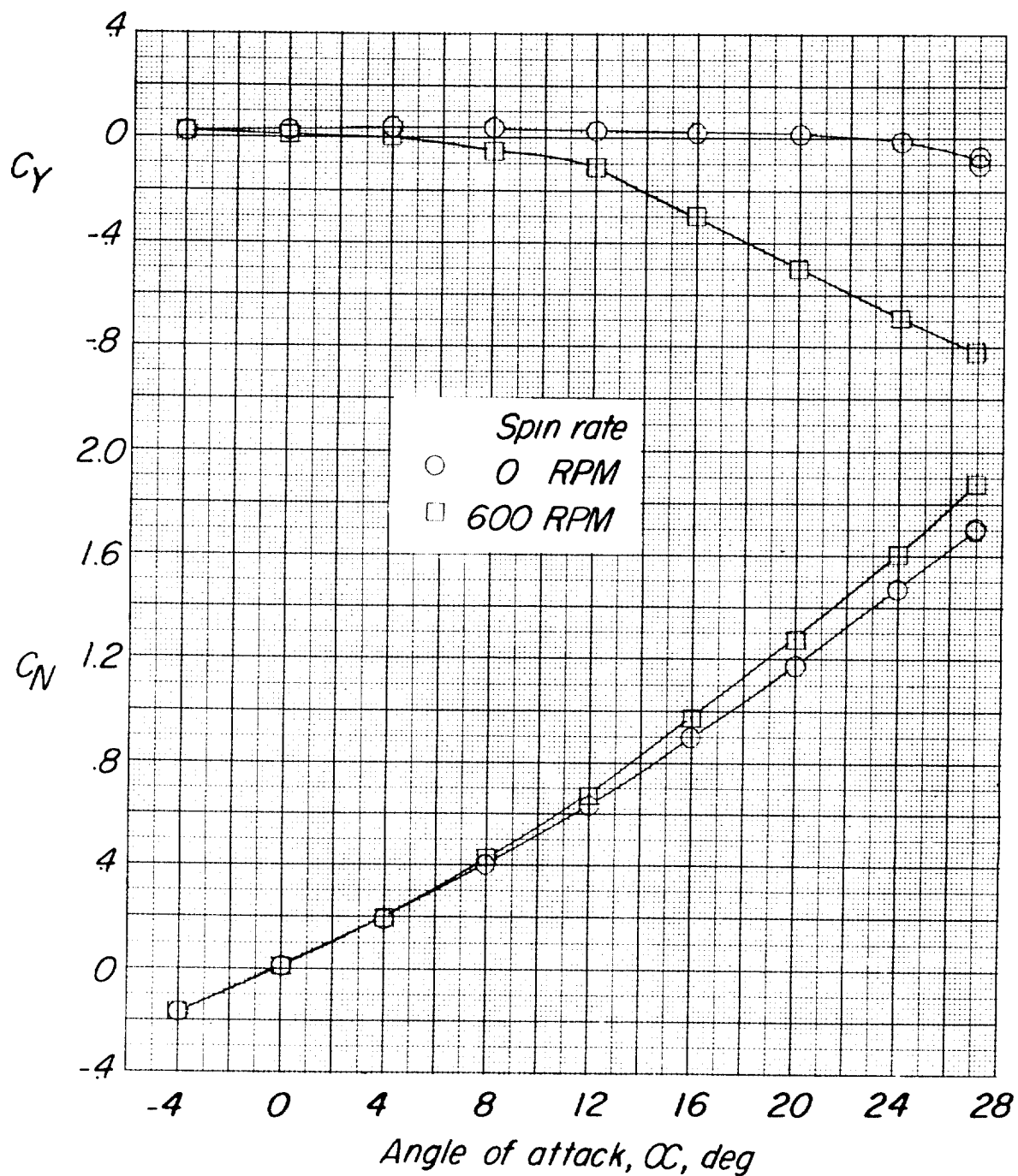


Figure 11.- Concluded.

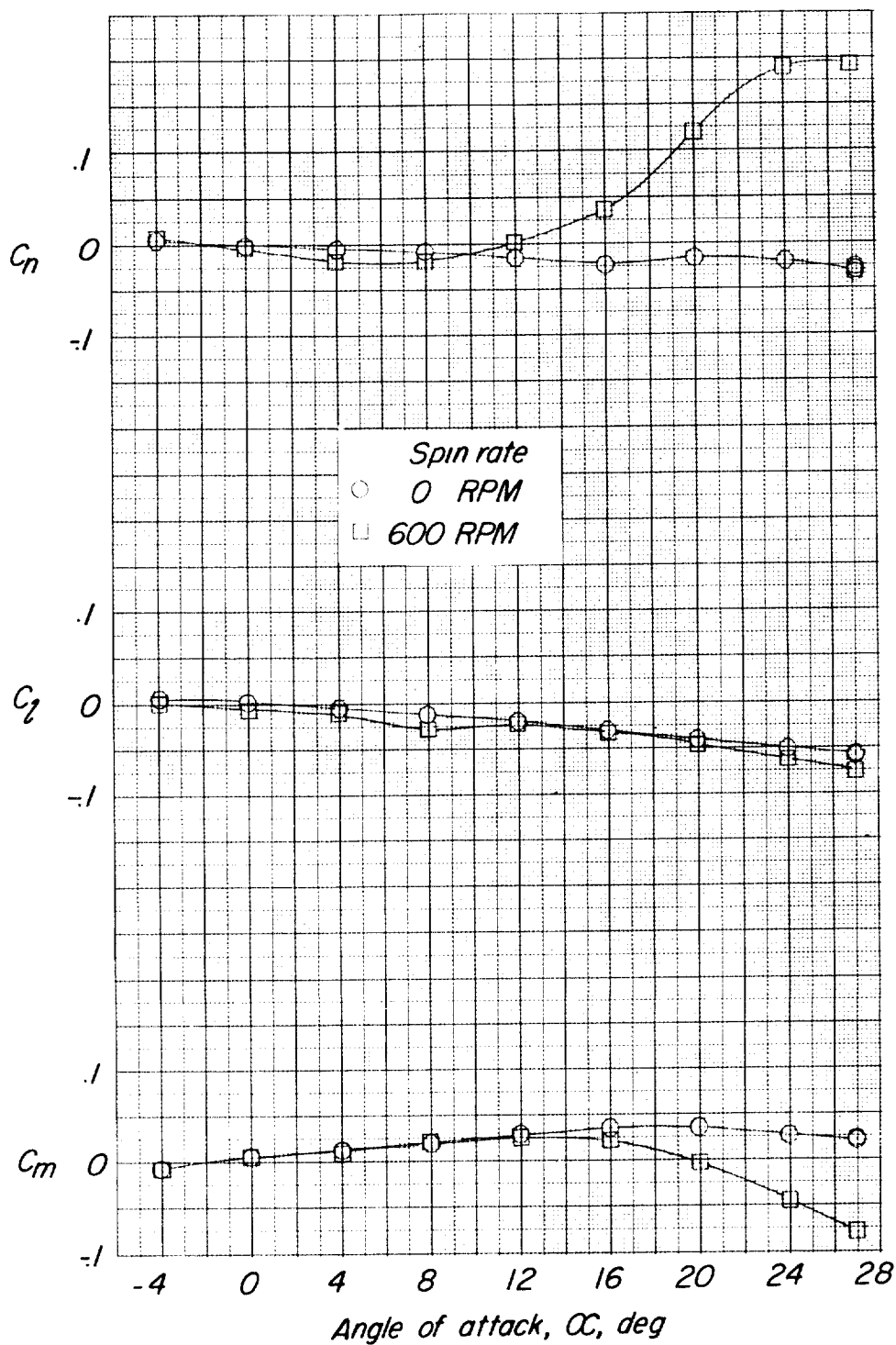


Figure 12.- Variation of the measured forces and moments against angle of attack in straight flow for two spin rates for the configuration with pointed nose and original tail.

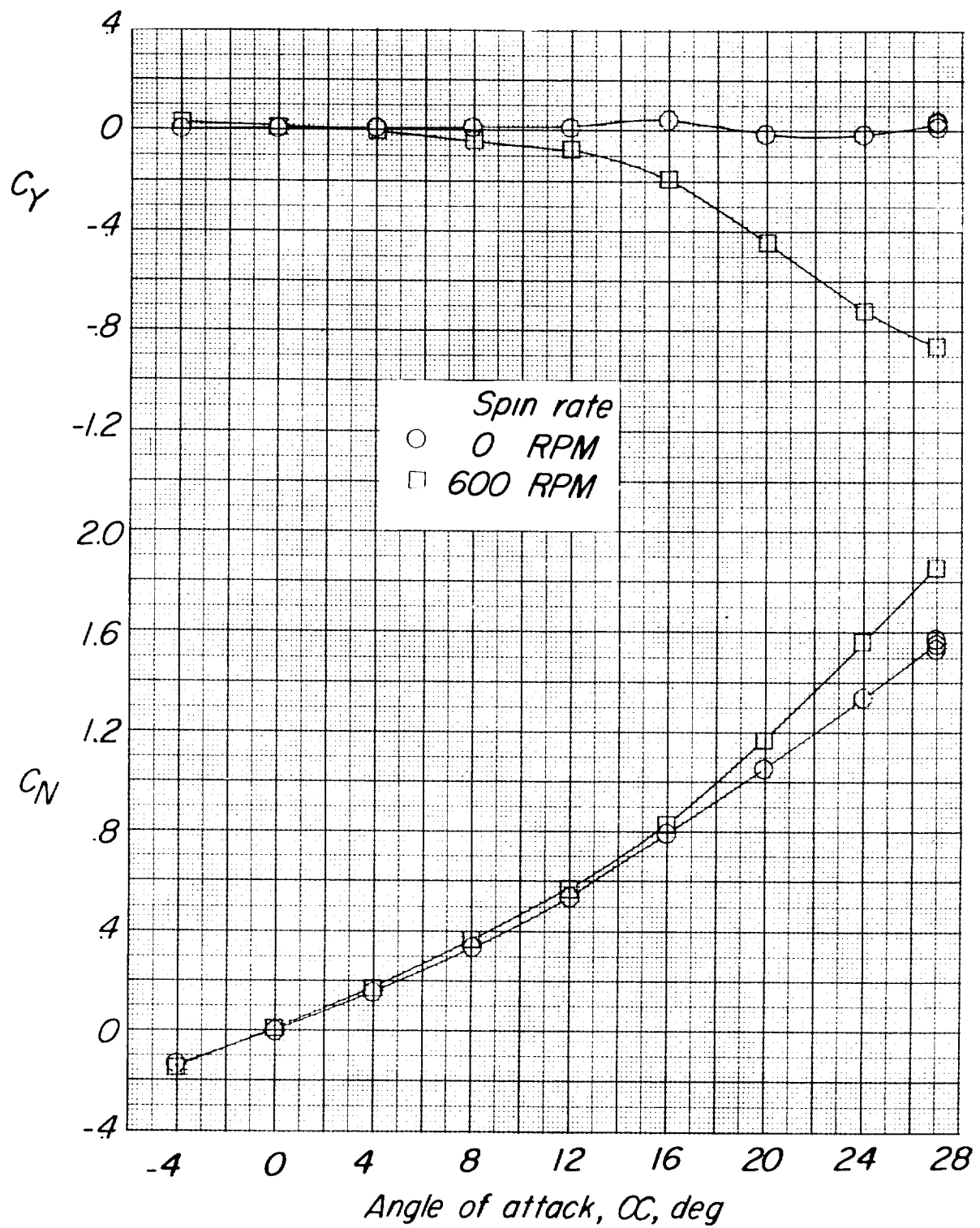


Figure 12.- Concluded.

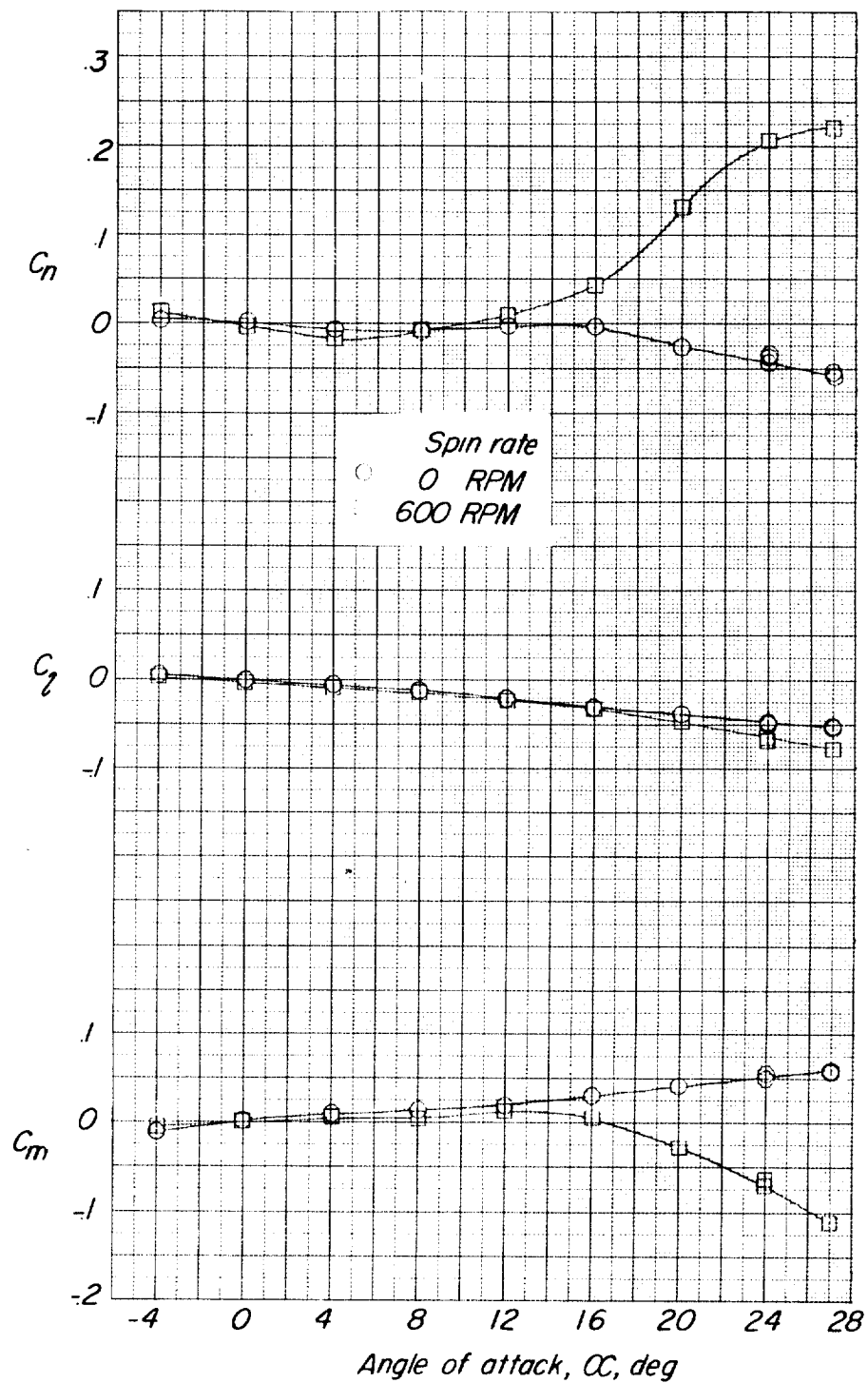


Figure 13.- Variation of the measured forces and moments against angle of attack in straight flow for two spin rates for the configuration with pointed nose and 6-fin tail.

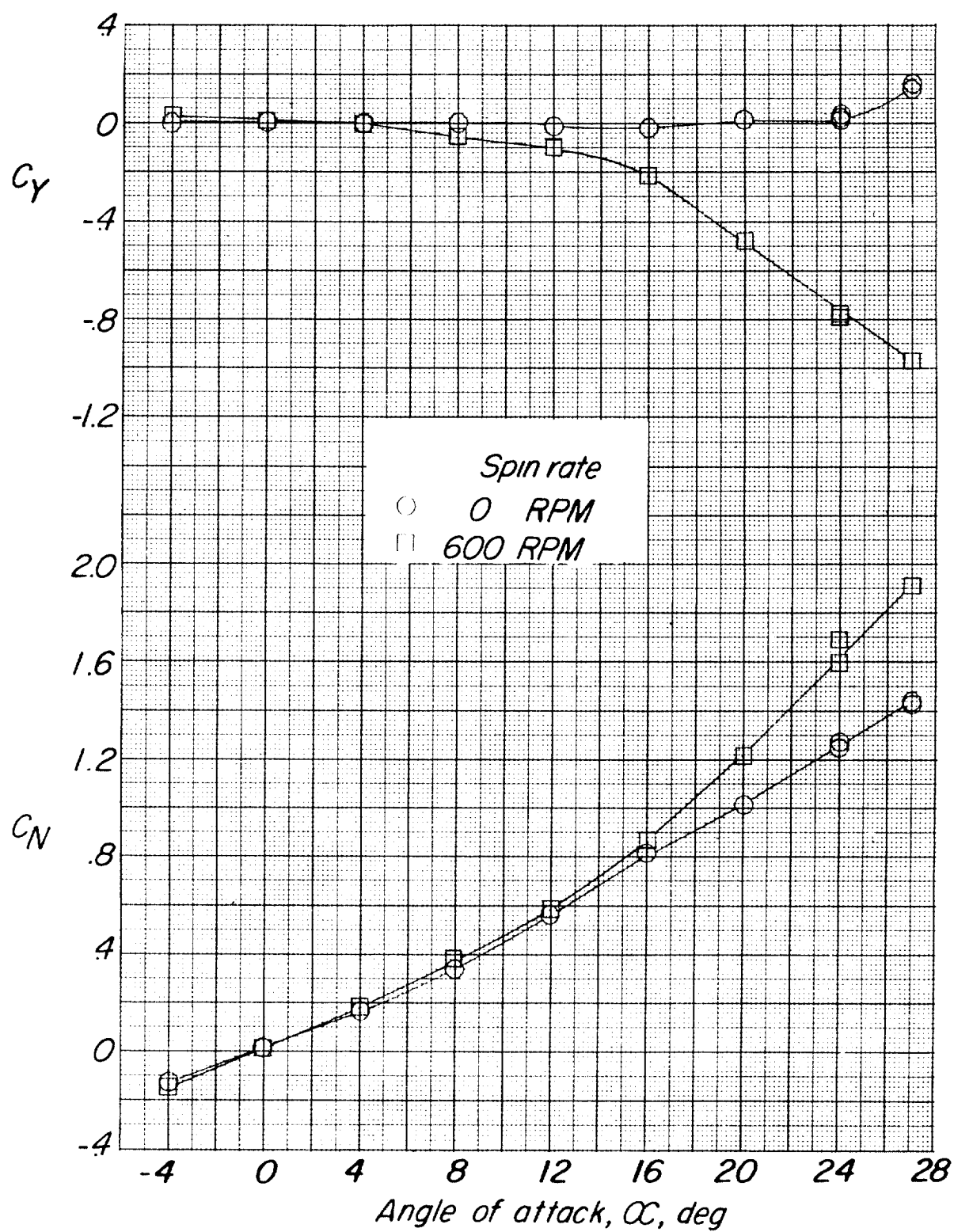


Figure 13.- Concluded.

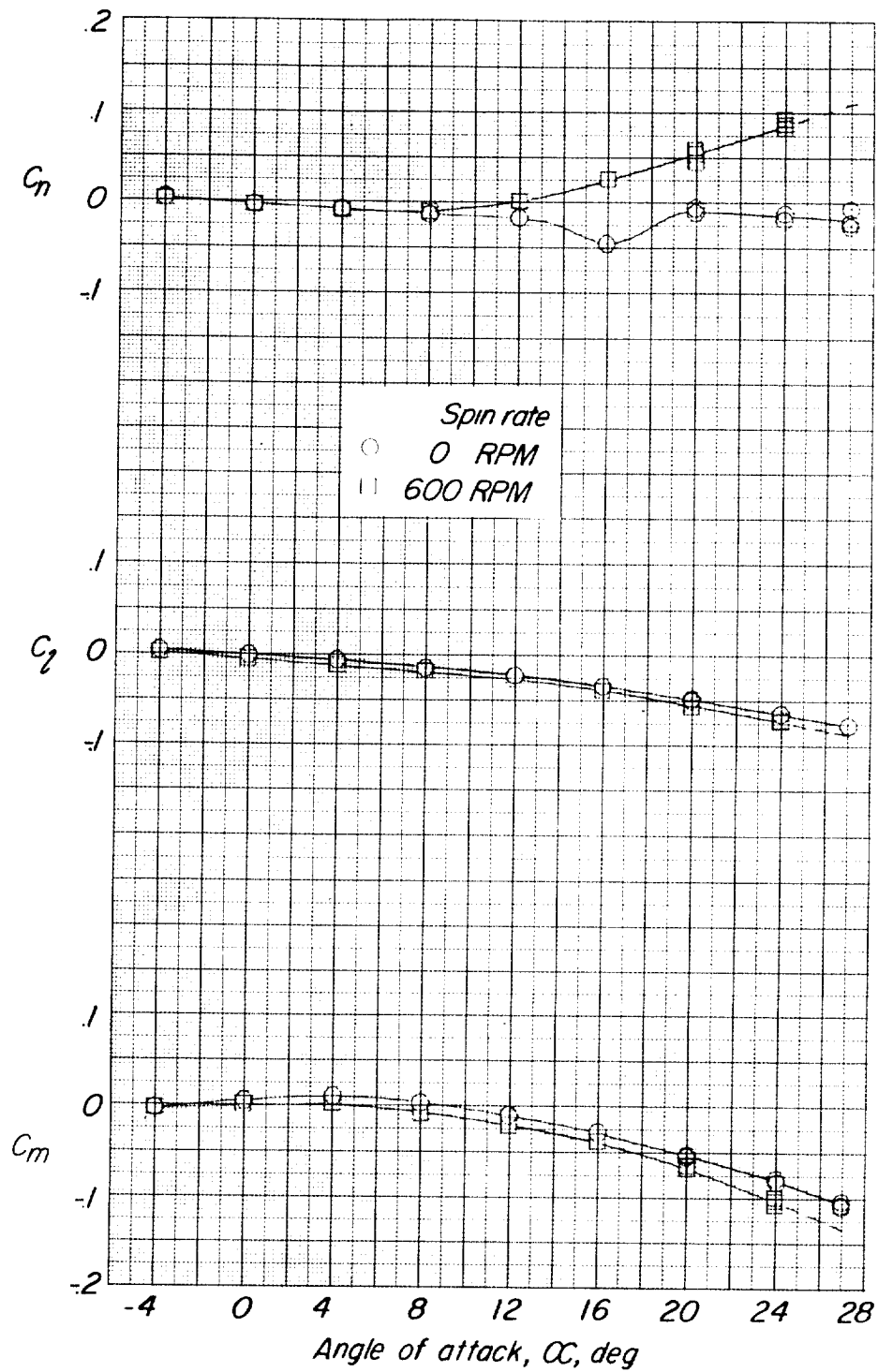


Figure 14.- Variation of the measured forces and moments against angle of attack in straight flow for two spin rates for the configuration with flat nose and original tail.

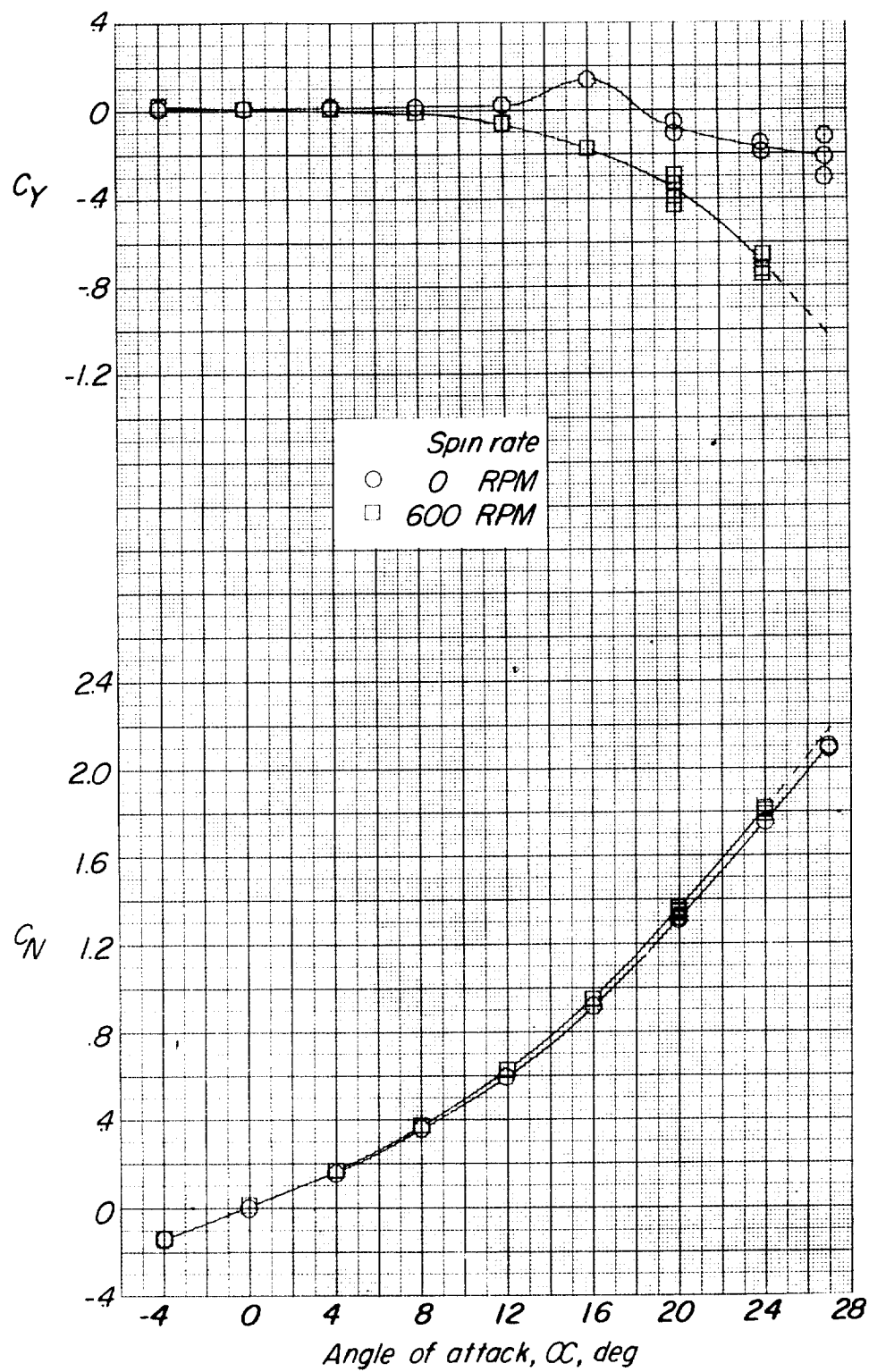


Figure 14.- Concluded.

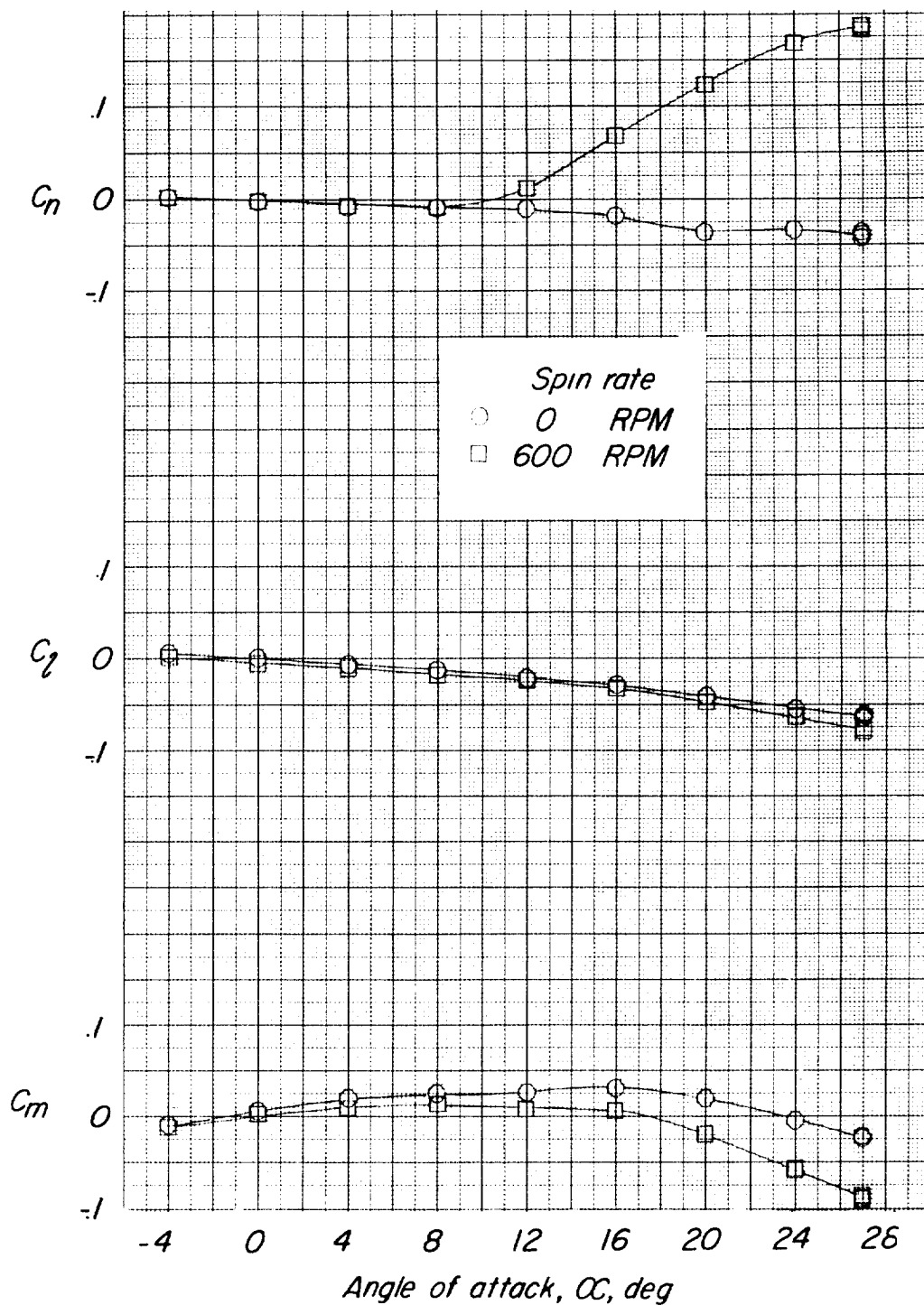


Figure 15.- Variation of the measured forces and moments against angle of attack in straight flow for two spin rates for the configuration with the original nose with ring spoiler and the original tail.

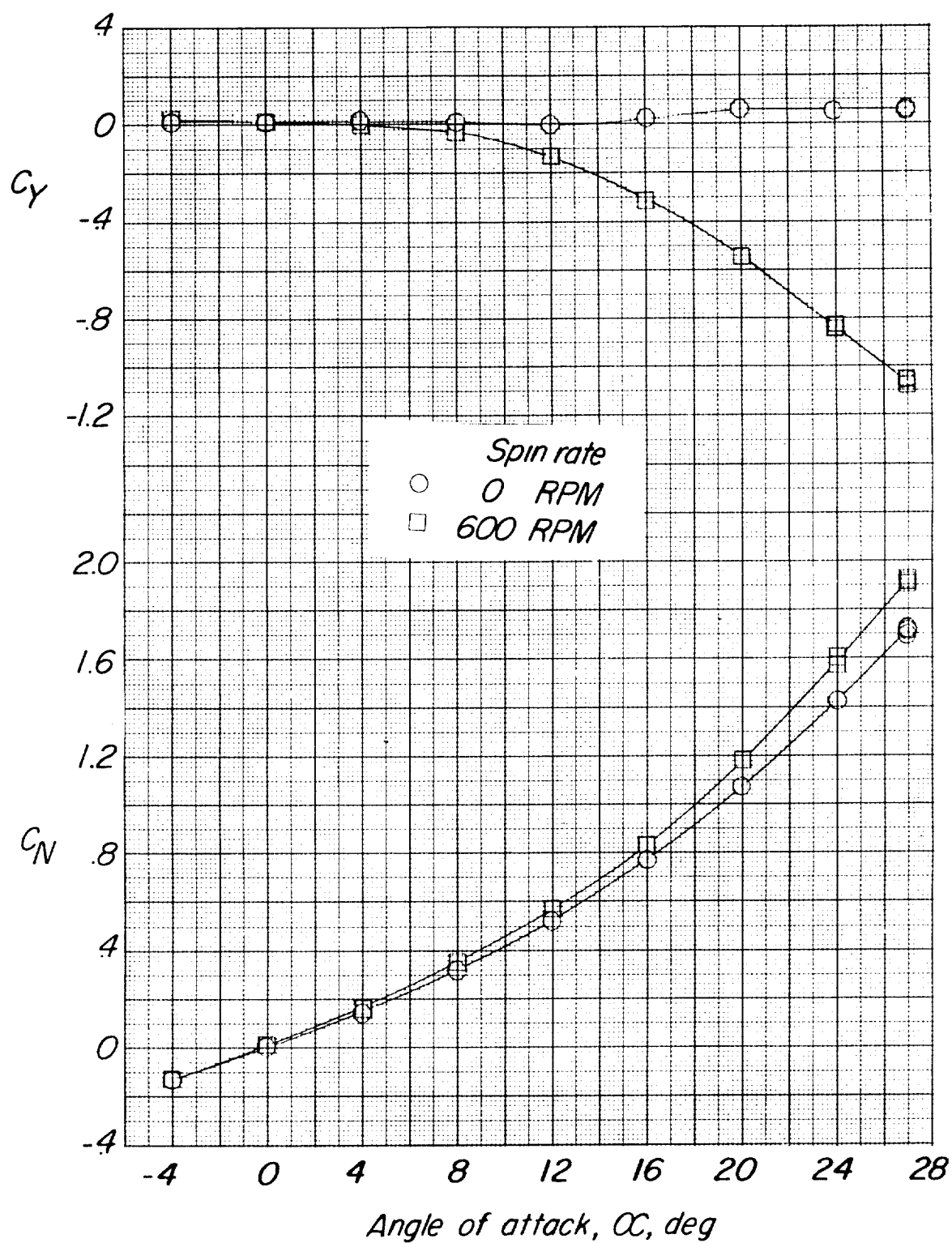
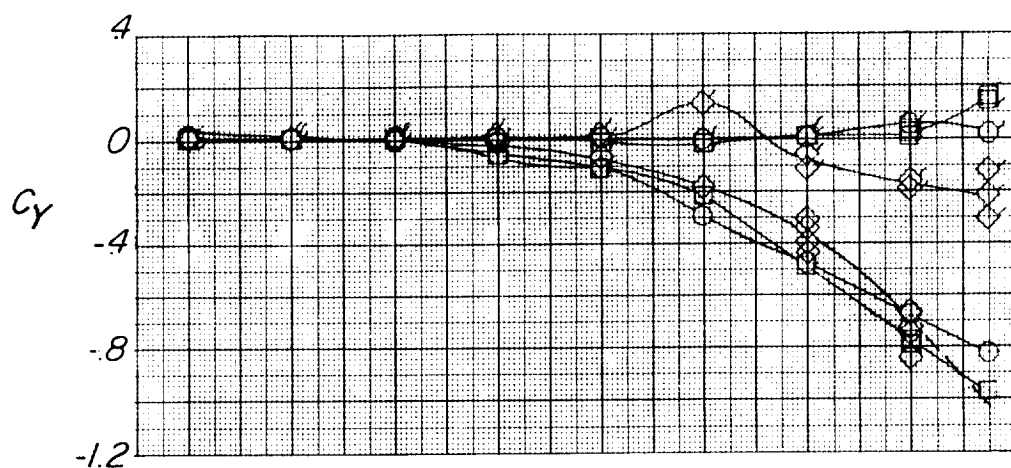


Figure 15.- Concluded.



Configuration	Spin rate, RPM	
	0	600
Original	○	○
Pointed nose, 6 fin tail	□	□
Flat nose, original tail	◇	◇

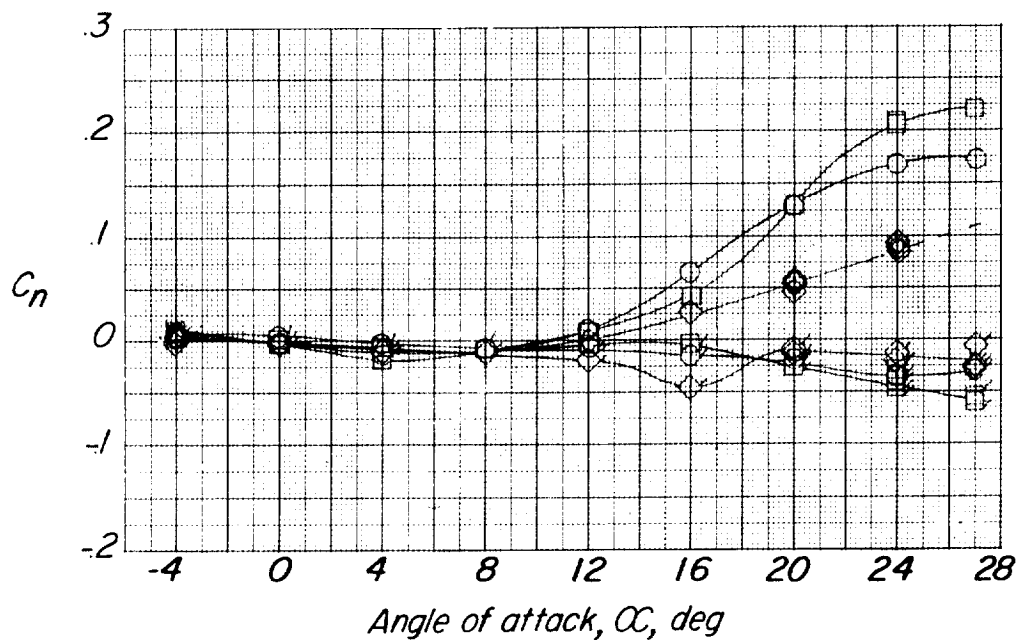


Figure 16.- Comparison of the Magnus force and moment for the original configuration with those having the largest and smallest Magnus effects.

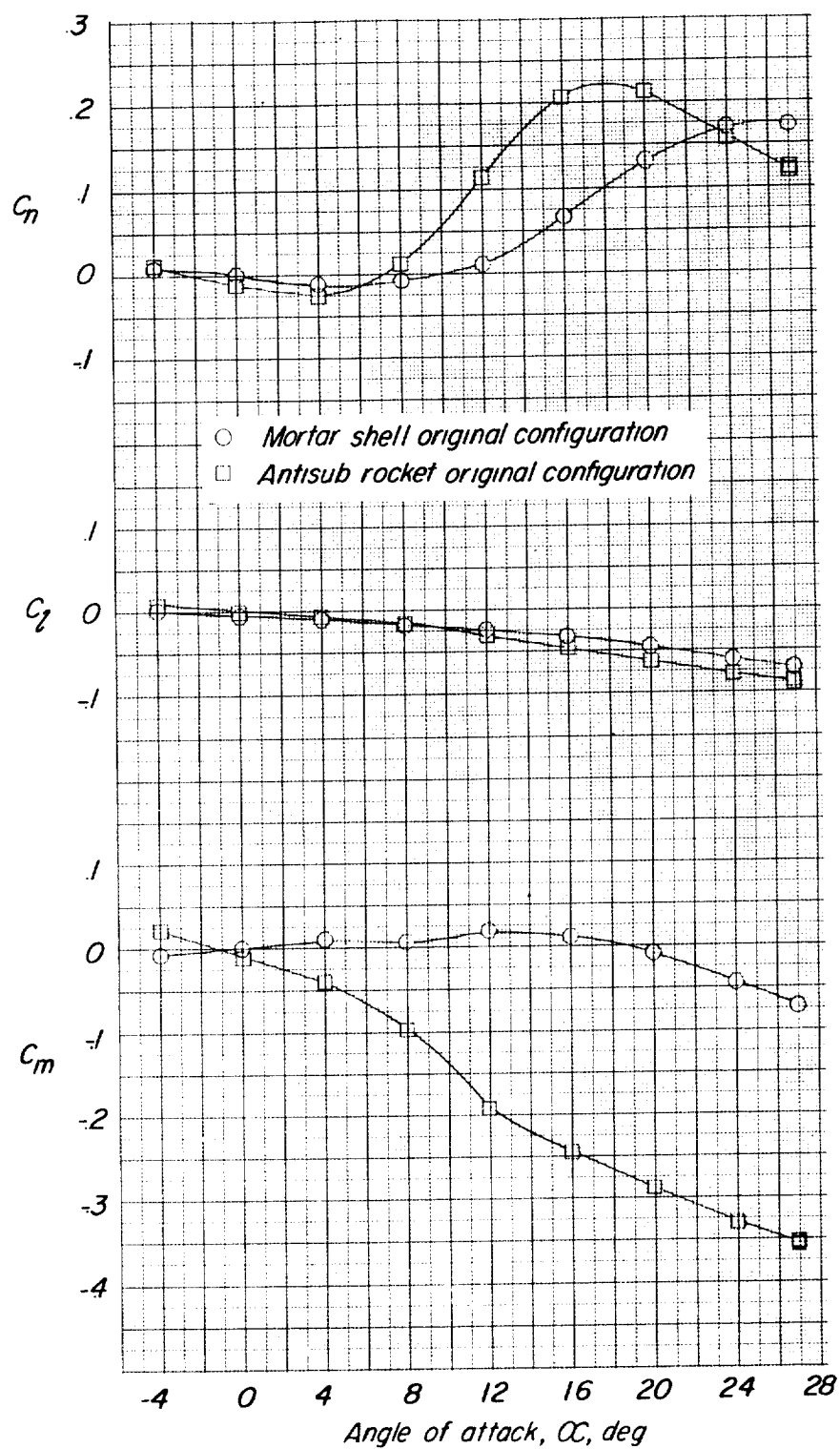


Figure 17.- Comparison of the mortar-shell data with the antisubmarine-rocket data from reference 7 and 600 rpm and for straight flow.

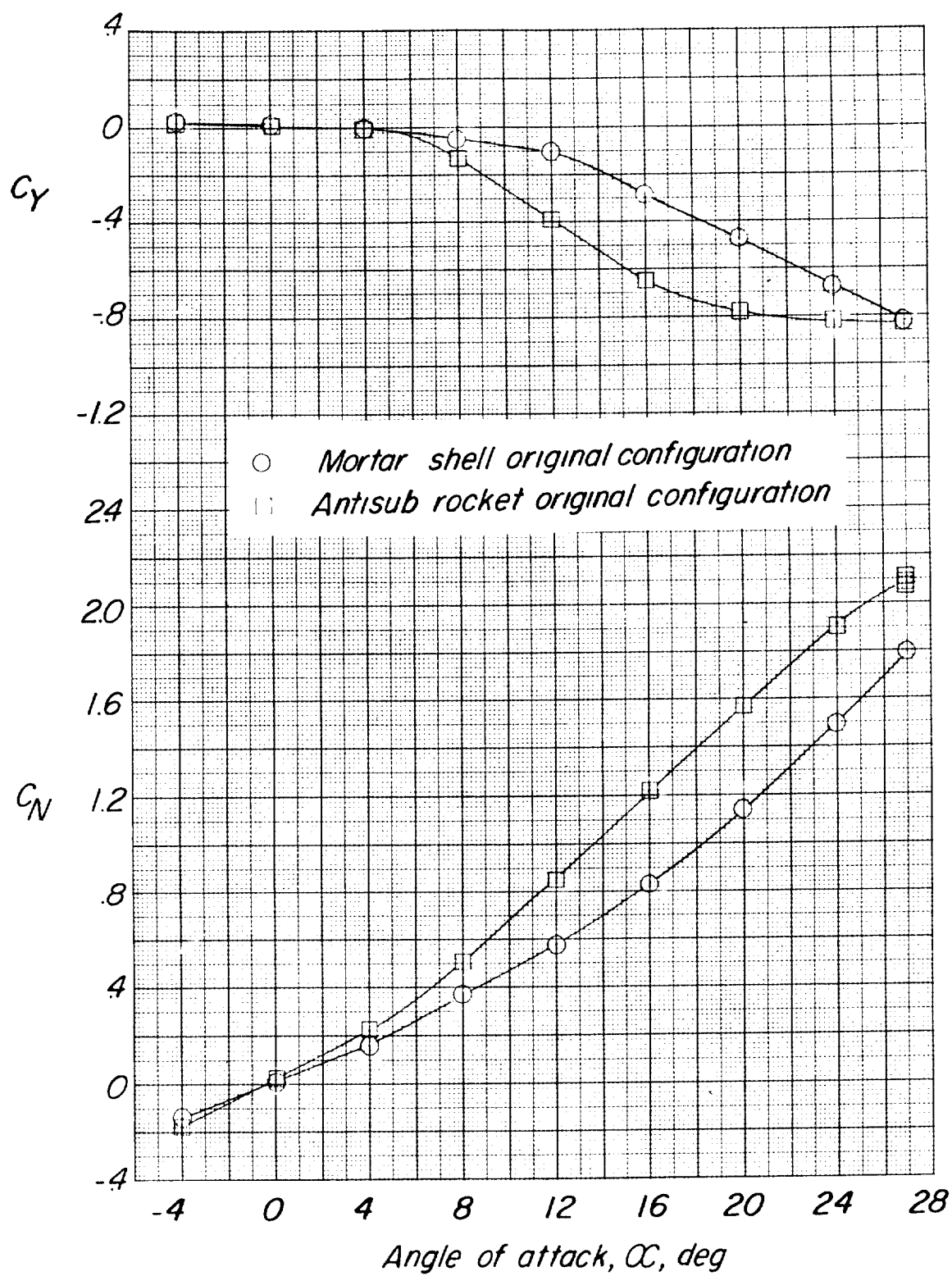
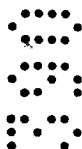


Figure 17.- Concluded.



A LOW-SPEED INVESTIGATION OF THE MAGNUS EFFECTS ON A
STING-MOUNTED MODEL OF A TYPICAL MORTAR SHELL

By Jacob H. Lichtenstein

ABSTRACT

An investigation has been made in the Langley stability tunnel with a 2.5-scale spinning model of a typical mortar shell. These tests were made to measure the aerodynamic forces and moments on a typical spinning mortar shell and were made in both straight and rolling flow for angles of attack up to 27° . It was found that variation of Magnus moment was nonlinear with angle of attack and that the directional stability was poor. This combination is potentially one that could give rise to a large-amplitude precessional motion.

INDEX HEADINGS

Bodies - Shape Variables	1.3.2
Tail-Body Combinations - Missiles	1.7.2.1.2
Missiles, Specific Types	1.7.2.2
Stability, Dynamic	1.8.1.2